Bulk Nanocrystalline Ferrite Stabilized through Grain Boundary Carbon Segregation

Yulia Ivanisenko,* Xavier Sauvage, Andrei Mazilkin, Askar Kilmametov, John A. Beach, and Boris B. Straumal

Bulk nanocrystalline ferrite with a grain size below 20 nm is stabilized thanks to grain boundary segregations of carbon atoms. This structure has been obtained through severe plastic deformation of a carbon steel containing only 0.45 wt% carbon with a bainitic microstructure. Both the mean grain size and resulting strength are similar to these obtained in pearlitic steels containing twice as much carbon and deformed in the same conditions. This indicates that very high strength can be achieved in nanocrystalline steels with much lesser carbon content.

Achieving ultrafine grained or nanocrystalline steels has been an important challenge during the past two decades. The main motivation is to take advantage of the Hall–Petch law that predicts strength of few GPa for grain sizes smaller than 100 nm.[1,2] Different strategies have been proposed including the use of bainitic transformation,[3,4] consolidation of nanocrystalline powders,[5] large levels of plastic deformation,[6,7] and crystallization of bulk metallic glasses.[8] The mechanical and

Dr. Y. Ivanisenko, Dr. A. Mazilkin, Dr. A. Kilmametov, Prof. B. B. Straumal
Karlsruhe Institute of Technology (KIT)
Institute of Nanotechnology
Hermann-von-Helmholtz-Platz 1, 76344 Eggenstein-Leopoldshafen
Germany
E-mail: julia.ivanisenko@kit.edu

Dr. X. Sauvage
Normandie Univ
UNIROUEN
INSA Rouen
CNRS
Groupe de Physique des Matériaux
76000 Rouen, France

Dr. A. Mazilkin, Prof. B. B. Straumal
Institute of Solid State Physics
Russian Academy of Sciences
Ac. Ossipyan str. 2, 142432 Chernogolovka, Russia

Dr. J. A. Beach
Department of Materials Science and Engineering
University of Illinois at Urbana-Champaign
USA

Prof. B. B. Straumal
National University of Science and Technology «MISIS»
Leninskii prosp. 4, 119049 Moscow, Russia

The ORCID identification number(s) for the author(s) of this article can be found under https://doi.org/10.1002/adem.201800443.

thermal stability of such nanoscaled structures is an issue and it has been shown that grain boundary (GB) segregations may play a key role,[9–11] while they could also affect significantly the mechanical properties.[12–14] In case of materials processed by severe plastic deformation (SPD),[4] it has also been shown that a small amount of solute interacting with crystalline defects may notably affect the dynamic recovery mechanisms and hence the final grain size.[15] The grain boundary segregation in nanograined materials can accommodate astonishing amounts of alloying agent atoms. For example, the solubility of cobalt in the wurtzite lattice of bulk ZnO at 500 °C is only ≈2 at%. In nanograined ZnO (grain size 20 nm) up to 40 at% Co can be dissolved.[16]

Following this idea and since it is known that carbon atoms are prone to GB segregation,[17] SPD processes sound attractive to achieve nanocrystalline steels. The solubility of carbon in alfa iron is, however, extremely limited[18] and only a martensitic structure with a poor ductility (i.e., not appropriate for SPD) may retain a significant carbon super saturated solid solution. However, it has been demonstrated that large levels of plastic deformation may give rise to cementite decomposition,[19–25] and it was proposed that the underlying mechanisms are driven by cementite fragmentation and carbon-dislocations or carbon-vacancies interactions.[19,21,26,27] Thus, pearlitic steels processed by heavy wire drawing[18,28] or high pressure torsion (HPT)[29–34] typically exhibit grain sizes in a range of 10–20 nm, with strong GB segregations of carbon, up to 1 at% C in solid solution[31,35,36] and remaining nanoscaled carbides and/or lamellar structures inherited from the original pearlitic structure. At the same time, it is interesting that only fine lamellar pearlite readily dissolves at SPD, whereas coarse and thick lamellar or spherical cementite dissolves in much lesser degree[30,33] being deformed in the same conditions.

The nanocrystalline microstructure of HPT-processed carbon steels demonstrate enhanced thermal stability as compared with that of martensite[37] and extremely high hardness also exceeding that of martensite. With such a complex microstructure, it is rather difficult to understand if these attractive properties of such steels simply result from a small grain size stabilized by GB segregations[9–11] or if the super saturated solid solution and remaining nanoscaled cementite particles also play a role.

In fact, it is interesting to note that the carbon content of such steels processed by SPD has never been optimized. A low energy electron diffraction study showed that segregated carbon atoms

occupy octahedral sites on the (100) plane as interstitials.[38] Let us consider a grain boundary with a square network of possible adsorption sites, spaced for $a = 0.26$ nm. Then on $1\,m^2$ about 15×10^{18} atoms can be accommodated. At first, we need to calculate the total grain boundary area S in $1\,m^3$ of steel with a grain size d of 15 nm. It can be done using the stereological equation[39]:

$$S = 2/d \qquad (1)$$

Therefore, the grain boundary area in $1\,m^3$ of steel with a grain size of 15 nm is $2/(15 \times 10^{-9}) = 1.33 \times 10^8\,m^2\,m^{-3}$. On this area $15 \times 10^{18} \times 1.33 \times 10^8 = 20 \times 10^{26}$ C atoms can be accommodated. This amount of C atoms corresponds to $20 \times 10^{26} \times 2 \times 10^{-23}\,g = 40$ kg of carbon. The density of the steel is $7800\,kg\,m^{-3}$. Therefore, one can accommodate approximately 0.5 wt% of carbon on grain boundaries in the steel with 15 nm grain size.
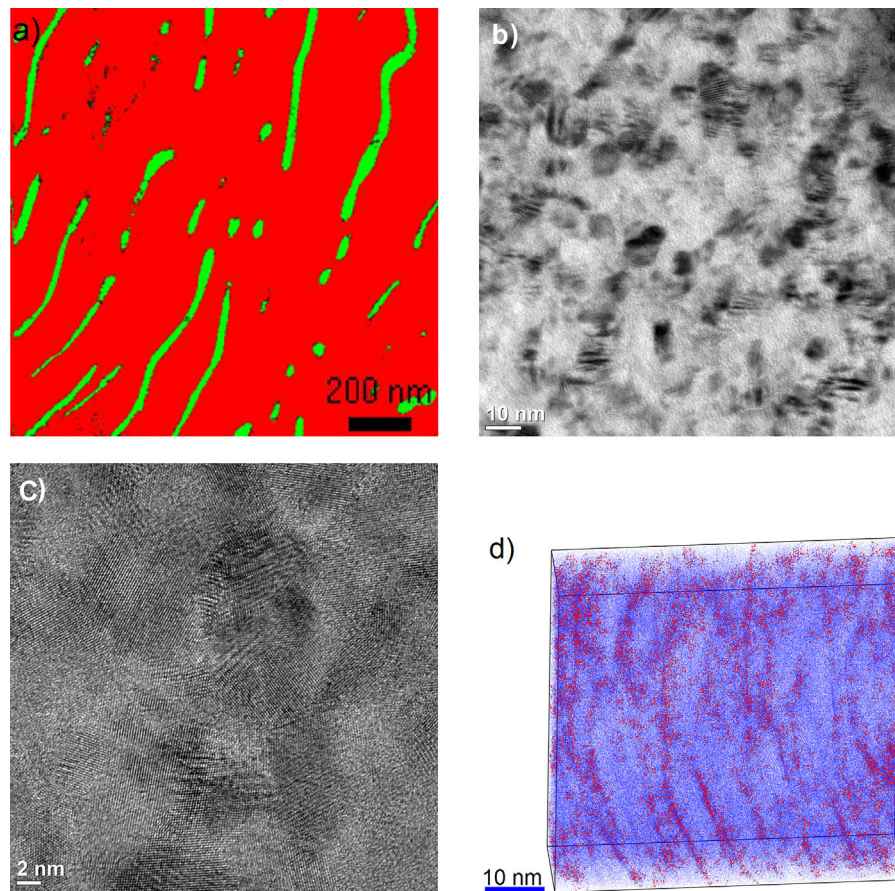
This amount approximately corresponds to the carbon content of a medium carbon steel like C45. This estimate shows that in order to stabilize the nanostructure of ferrite we need much less carbon than it contains in eutectoid steel!

In the present work, we purposely used strain induced cementite dissolution in a steel with a carbon content near 2 at% (0.45 wt%) in order to address the following questions: 1) whether it is possible to produce the nanocrystalline structure in a carbon steel in which all carbon is distributed along/segregated at the grain boundaries, and what is the mechanism of such grain boundary segregations formation? 2) which maximal strength can be achieved in a nanocrystalline steel without contributions of such strengthening mechanisms as the formation of martensite and precipitation hardening?

A commercial Fe–0.45 wt%C–0.5 wt%Mn steel (C45) has been subjected to a patenting treatment as described in ref. [40] to achieve a fine scale bainitic structure with a homogeneous distribution of nanoscaled lamellar cementite. Ø10 mm rods were then sliced by spark erosion to obtain 0.2 mm thick discs for the HPT process (HPT machine from W. Klement GmbH, Lang, Austria with Bridgman anvils made of tungsten carbide). Five revolutions under a pressure of 7 GPa were carried out at room temperature and at a rotation rate of 1 rpm. Samples for structural investigations were cut at a distance of 3 mm from the center corresponding to a shear strain of 300. Microstructures were characterized by transmission electron microscopy (TEM) on a TITAN (200 kV) microscope with Cs correction using samples prepared by the focused ion beam (FIB) technique, and for Automated Crystal Orientation Mapping (ACOM) acquisition the FEI Tecnai F20 operated at 200 kV and equipped with an ASTAR system were used. Orientation maps have been obtained with an acquisition speed of 100 frames per second. Atom probe tomography (APT) analyses were performed with a LEAP 4000-HR. Samples were field evaporated at 80 K using electric pulses (20% pulse fraction, repetition rate of 200 kHz). Three dimensional reconstructions were computed using IVAS software and further data processing was carried out with the GPM_3Dsoft. APT samples were prepared by conventional electropolishing methods. High resolution synchrotron diffraction data were collected using beamline 11-BM at the Advanced Photon Source (APS), Argonne National Laboratory using an average wavelength of 0.414580 Å. Discrete detectors covering an angular range from -6 to $16°$ 2 theta are scanned over a $34°$ 2 theta range, with data points collected every $0.001°$ 2 theta and scan speed of $0.1°\,s^{-1}$. Measurements were collected from the samples using a transmission geometry over a 2 mm square area. Lattice parameters were derived using the Rietveld refinement and Fityk software. The microhardness was measured in the HPT sample locations corresponding to a distance of 3 mm from the center at a load of 500 g using a Buehler Micromet 5104 tester. Samples were carefully polished before hardness measurements.

In the initial as-patented state, the microstructure of the steel consisted of the mixture of ferrite and cementite lamellae, with the average thickness of 200 and 13 nm, respectively (**Figure 1**a). After HPT the microstructure of the steel was refined down to a nanometer range, and ACOM TEM technique could not be applied. Bright field TEM image (Figure 1b) clearly shows that a homogeneous nanocrystalline structure has been achieved by SPD. It is supported by high resolution TEM images (in Figure 1c). Such structure is apparently similar to that of pearlitic steels (0.8 wt% C) processed by HPT.[29,32] Similarly to 0.8 wt% steel reported in ref. [29], the mean grain size of ferrite, estimated using a number of dark field images, is between 10 and 20 nm, which is in a good agreement with HRTEM image in Figure 1b. The carbon distribution was investigated by APT and a thin section of the analyzed volume shown on Figure 1d shows qualitatively that carbon atoms are not homogeneously distributed in this structure but have segregated along crystalline defects, which are most probably grain boundaries. In facts elongated depleted regions 10 to 15 nm in thickness are surrounded by extended carbon layers containing between 4 and 8 at% C. These layers are relatively thick, up to several nanometers, which is thicker than accepted grain boundary thickness of 0.5 nm. We propose that carbon can also segregate to dislocations which always present with a high density close to GBs in severely deformed materials.[41,42] According to Bhadeshia,[43] in the presence of dislocations rather high carbon concentrations may exist without a change in lattice parameter of ferrite. Also one should note that this apparent thickness might also be affected by local magnification effects[44] and overestimated due to the intersection angle between the GB surface and the plane used to compute the composition map. Further details of this distribution will be discussed later in this manuscript, but it is important to note that the carbon concentration in the whole analyzed volume is 2.7 ± 0.2 at% (so, very close to the nominal composition) and that no cementite particle could be detected. Thus, it indicates that carbides have been dissolved during SPD. The XRD pattern of the patented steel before deformation is compared to that of the material after HPT in **Figure 2**a. Cementite diffraction peaks, clearly seen in as-patented state, cannot be identified out of the background after HPT (Figure 2c). It is consistent with APT data and confirms the dissolution of cementite during SPD. Note that the XRD pattern of the HPT-processed specimen contains also reflections of tungsten carbide, that is, the material of anvils used for HPT processing (Figure 2c). Therefore some WC particles embedded into the sample during severe straining. Concerning peaks attributed to ferrite, a uniform shift to low diffraction angles is clearly exhibited (Figure 2b). This shift is connected to

**ADVANCED
SCIENCE NEWS**
www.advancedsciencenews.com

**ADVANCED
ENGINEERING
MATERIALS**
www.aem-journal.com

Figure 1. Microstructure of the C45 steel in the initial as patented state, two-phase ACOM TEM image, ferrite appears red, and cementite green a) and deformed by HPT to equivalent shear strain $\gamma \approx 300$: b) bright field image; c) high resolution TEM image showing nanocrystalline grains of ferrite; d) 3D reconstructions of a volume analyzed by APT ($60 \times 15 \times 60\,nm^3$–the shear plane is vertical) showing the distribution of Fe (blue) and C atoms (red). To outline the heterogeneous distribution of carbon, data have been filtered to keep only carbon atoms in regions where the concentration was higher than 3.5 at%. (For interpretation of the references to color in this figure legend, the reader is referred to the web version of this article).

an increase of the lattice parameter of ferrite from $0.28668 \pm 0.00001\,nm$ in the patented structure to $0.28696 \pm 0.00001\,nm$ after HPT, upon that lattice remains cubic, and does not become tetragonal.

According to ref. [45], the estimated values of lattice parameters correspond to 0.1 and 0.3 at% (0.02 and 0.065 wt%) of carbon in solid solution in ferrite, respectively. This is significantly less than the nominal composition, confirming GB segregations pointed out by APT data (Figure 1d).
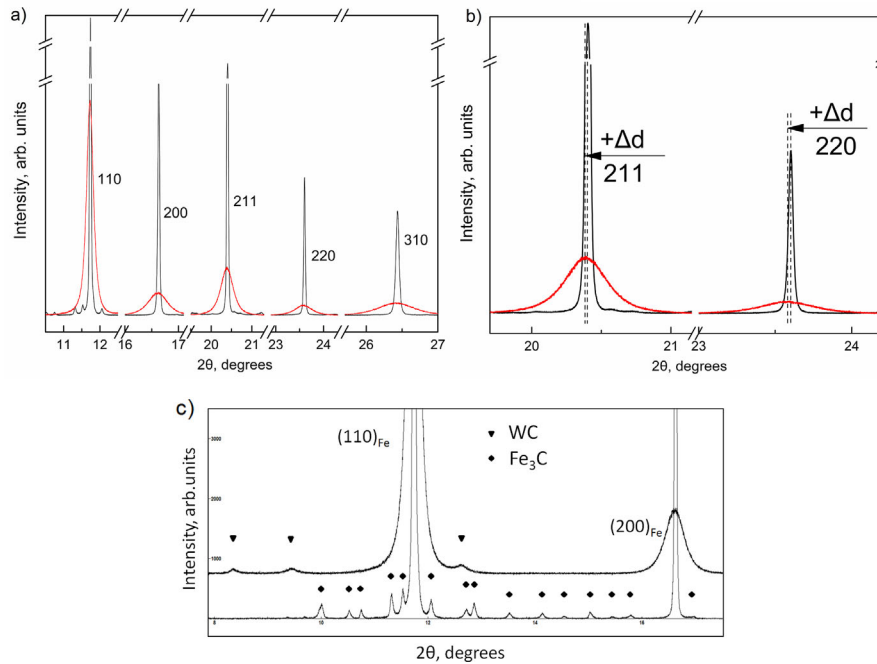
In principle, it is also possible to quantitatively determine directly the amount of carbon in solid solution from APT data. However, considering GB segregations and the very small grain size the following procedure has been followed. Data have been first filtered using the "isoposition" procedure (see ref. [44] for details) with different thresholds to keep only atoms in carbon-poor regions (**Figure 3**). As expected, the number of atoms remaining after the filtering procedure increases with the increasing threshold (red curve) and the corresponding carbon concentration also (blue curve). The theoretical fraction of atoms inside grains simply writes as:

$$X = (D - t_{ap})^3 / D^3 \qquad (2)$$

For a grain size D of 10 nm and an apparent GB thickness t_{ap} (as it appears in APT volume) in a range of 2 to 3 nm, then $30\% < X < 50\%$. As shown on Figure 3, this ratio is obtained by filtering with a threshold in a range of 2–2.5 at% and it gives a carbon concentration in a range of 0.2–0.5 at% C (0.04 to 0.1 wt%) in solid solution which is rather consistent with XRD data.

The hardness of HPT-processed C45 steel was 903 ± 40 HV, which is very close to 940 HV reported for a fully pearlitic steel with 0.8 wt%C.[37]

Thus, after SPD, the nanocrystalline structure is characterized by a grain size of 15 ± 5 nm with GBs covered by a large proportion of carbon atoms, only a small fraction being in solid solution (0.065 wt% according to XRD). Upon that the ferrite crystallite lattice remains cubic which is not consistent with the data reported by Djaziri et al.[28] for a pearlitic steel drawn to a true strain of 2. These authors have shown that some tetragonality already starts to appear for such carbon content in solid solution. The reason for the increased dissolution of carbon in the ferrite lattice and for the formation of tetragonal distortions after drawing could be related with the specific stress distribution in the wire during the drawing process. Due to the

**ADVANCED
SCIENCE NEWS**

www.advancedsciencenews.com

**ADVANCED
ENGINEERING
MATERIALS**

www.aem-journal.com

Figure 2. a) XRD patterns of the C45 steel after patenting treatment (black) and subsequent HPT (red lines); b) enlarged portion of XRD patterns shown in a), shift of XRD peaks due to carbon dissolution in ferrite lattice is indicated; c) The XRD pattern of C45 steel after patenting treatment (lower curve) and subsequent HPT (upper curve). Note numerous cementite reflections present in the initial as-patented state, which completely absent after HPT. (For interpretation of the references to color in this figure legend, the reader is referred to the web version of this article).

presence of strong wire texture <110> // to drawing direction/wire axis, extension stresses lead to the (elastic) expansion of the lattice in <110> direction and thus facilitate the occupation with C of the octahedral lattice sites with favorable positions. Djaziri et al.,[28] suggested that elastic strains of 1–2% achieved in the drawn wire during the drawing process are mostly responsible for the formation of tetragonal distortions. Let us note that at HPT of C45 steel such level of elastic stresses is also conceivable (taking into account its hardness of 900 HV and corresponding yield strength of 3 GPa), but no tetragonality was observed. In

case of HPT deformation with simple shear stress-strain conditions, shear texture forms with several partial fibers, it is much weaker as compared with that resulting from wire drawing. Therefore, there is no preferable sites for C atoms, they occupy them randomly and lead to uniform expansion of cubic lattice.

In order to explain the formation of grain boundary segregations with such a high concentration of carbon in C45 steel as a result of HPT, we propose the following scenario. During severe shearing ferrite lamellae align in shear direction and get thinner and thinner with increasing strain.[29] Simultaneously, transverse grain boundaries appear due to storage of geometrically necessary dislocations, leading to the formation of almost equiaxed grains of ferrite (Figure 1c). Cementite lamellae also deform plastically remaining between the ferrite ones. In that way, interphase area increases drastically and cementite lamellae represent carbon depots from which carbon can spread along the percolating network of ferrite grain boundaries. It has been shown that already in the beginning of HPT processing cementite becomes nanocrystalline with crystals in the size range of 5–20 nm.[46] There are several experimental evidences showing that severe deformation leads to the amorphyzation of cementite.[35,47,48] The reason for that can be depletion of cementite with carbon/formation of non-stoichiometric cementite[49] or strong stresses acting on cementite from the ferrite phase.[47] This should further facilitate spreading of carbon from amorphous cementite along the interfaces at continuing straining. In that way carbon segregations naturally form along the ferrite grain boundaries at HPT. In fact, extended surface-like carbon segregations with the concentration of 6–8 at% periodically distributed in the
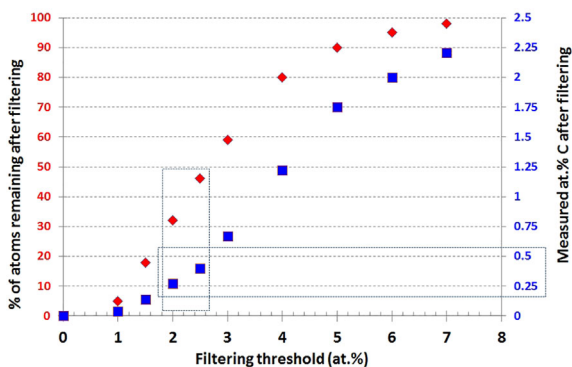
Figure 3. Percentage of atoms remaining in the analyzed volume (red curve) and measured carbon concentration (blue curve) as a function of the carbon threshold selected (see text for details). (For interpretation of the references to color in this figure legend, the reader is referred to the web version of this article).

microstructure at the distances comparable with the ferrite grain size (Figure 1d) represent the rests of cementite lamellae. Relatively small amount of carbon found in ferrite lattice can result from the dislocation-assisted diffusion processes, as discussed before.[21,29] This mechanism also explains well why coarse-lamellar or spherical cementite does not dissolve at severe deformation. In both these cases plastic deformation of cementite is difficult, as only fine lamellae of cementite can plastically deform as it was established earlier by Langford.[50]

The nanostructure of C45 steel formed in this way, where carbon is mostly segregated to grain boundaries and dislocations in close vicinity to grain boundaries demonstrates higher hardness as compared with that of martensite in steel with 0.8 wt%C, and similar hardness as in that steel after HPT processing.[37] The latter fact suggests that very high hardness can be obtained with lesser amount of carbon, because grain boundary strengthening provides the main contribution. Furthermore, nanostructured ferrite with GB segregations has increased thermal stability in comparison with quenched martensite.[37]

The performed investigations allowed to conclude that the microstructure of nanostructured ferrite with practically all carbon segregated to grain boundaries observed in C45 steel at high pressure torsion forms as a result of severe shearing of initial ferrite and cementite lamellae. Such microstructure demonstrates higher hardness than martensite in steel with 0.8 wt%C, and is comparable/similar to that of steel with 0.8 wt%C after HPT processing. This indicates that using severe plastic deformation very high mechanical properties can be obtained in steels with lesser carbon content, whether the initial state had a fine-pearlitic or bainitic microstructure.

Acknowledgements

Conflict of Interest

The authors declare no conflict of interest.

Keywords

[1] G. Saada, *Mater. Sci. Eng. A* **2005**, *400–401*, 146.

[2] V. Bata, E. V. Pereloma, *Acta Mater.* **2004**, *52*, 657.

[3] C. N. Hulme-Smith, S. W. Ooi, H. K. D. H. Bhadeshia, *Metall. Mater. Trans. A* **2017**, *48*, 4957.

[4] F. G. Caballero, H. K. D. H. Bhadeshia, K. J. A. Mawella, D. G. Jones, P. M. Brown, *Mater. Sci. Technol.* **2002**, *18*, 279.

[5] H. W. Zhang, R. Gopalan, T. Mukai, K. Hono, *Scr. Mater.* **2005**, *53*, 863.

[6] J. D. Embury, R. M. Fisher, *Acta Metall.* **1966**, *14*, 147.

[7] D. Raabe, P. Choi, Y. Li, A. Kostka, X. Sauvage, F. Lecouturier, K. Hono, R. Kirchheim, R. Pippan, D. Embury, *MRS Bull.* **2010**, *35*, 982.

[8] M. von Heimendahl, G. Maussner, *J. Mater. Sci.* **1979**, *14*, 1238.

[9] R. Kirchheim, *Acta Mater.* **2007**, *55*, 5129.

[10] R. Kirchheim, *Acta Mater.* **2007**, *55*, 5139.

[11] A. R. Kalidindi, C. A. Schuh, *Acta Mater.* **2017**, *132*, 128.

[12] V. G. Gavriljuk, *Scr. Mater.* **2005**, *52*, 951.

[13] J. Hu, Y. N. Shi, X. Sauvage, G. Sha, K. Lu, *Science* **2017**, *355*, 1292.

[14] K. Edalati, T. Masuda, M. Arita, M. Furui, X. Sauvage, Z. Horita, R. Z. Valiev, *Sci. Rep.* **2017**, *7*, 2662.

[15] H. W. Zhang, X. Huang, R. Pippan, N. Hansen, *Acta Mater.* **2010**, *58*, 1698.

[16] B. B. Straumal, S. G. Protasova, A. A. Mazilkin, E. Goering, G. Schütz, P. B. Straumal, B. Baretzky. *Beilstein J. Nanotechnol.* **2016**, *7*, 1936.

[17] J. Takahashi, K. Kawakami, K. Ushioda, S. Takaki, N. Nakata, T. Tsuchiyama, *Scr. Mater.* **2012**, *66*, 207.

[18] Y. Li, D. Raabe, M. Herbig, P.-P. Choi, S. Goto, A. Kostka, H. Yarita, C. Borchers, R. Kirchheim, *PRL* **2014**, *113*, 106.

[19] V. N. Gridnev, V. G. Gavriljuk, *Phys. Met.* **1982**, *4*, 531.

[20] W. Lojkowski, M. Djahanbakhsh, G. Burkle, S. Gierlotka, W. Zielinski, H.-J. Fecht, *Mater. Sci. Eng. A* **2001**, *303*, 197.

[21] X. Sauvage, J. Copreaux, F. Danoix, D. Blavette, *Philos. Mag.* **2000**, *4*, 781.

[22] K. Hono, M. Ohnuma, M. Murayama, S. Nishida, A. Yoshie, T. Takahashi, *Scr. Mater.* **2001**, *44*, 977.

[23] Y. J. Li, P. Choi, C. Borchers, S. Westerkamp, S. Goto, D. Raabe, R. Kirchheim, *Acta Mater.* **2011**, *59*, 3965.

[24] S. Ohsaki, K. Hono, H. Hidaka, S. Takaki, *Scr. Mater.* **2005**, *52*, 271.

[25] X. Sauvage, W. Lefebvre, C. Genevois, S. Ohsaki, K. Hono, *Scr. Mater.* **2009**, *60*, 1056.

[26] C. Borchers, Y. Chen, M. Deutges, S. Goto, R. Kirchheim, *Philos. Mag. Lett.* **2010**, *90*, 581.

[27] G. A. Nematollahi, J. von Pezold, J. Neugebauer, D. Raabe, *Acta Mater.* **2013**, *61*, 1773.

[28] S. Djaziri, Y. Li, G. A. Nematollahi, B. Grabowski, S. Goto, C. Kirchlechner, A. Kostka, S. Doyle, J. Neugebauer, D. Raabe, G. Dehm, *Adv. Mater.* **2016**, *28*, 7753.

[29] Y. Ivanisenko, W. Lojkowski, R. Z. Valiev, H.-J. Fecht, *Acta Mater.* **2003**, *51*, 5555.

[30] V. A. Shabashov, L. G. Korshunov, A. G. Mukoseev, V. V. Sagaradze, A. V. Makarov, V. P. Pilyugin, S. I. Novikov, N. F. Vildanova, *Mater. Sci. Eng. A* **2003**, *346*, 196.

[31] X. Sauvage, Y. Ivanisenko, *J. Mater. Sci.* **2007**, *42*, 1615.

[32] Y. Ivanisenko, I. MacLaren, X. Sauvage, R. Z. Valiev, H.-J. Fecht, *Acta Mater.* **2006**, *54*, 1659.

[33] B. B. Straumal, A. A. Mazilkin, S. G. Protasova, S. V. Dobatkin, A. O. Rodin, B. Baretzky, D. Goll, G. Schütz, *Mater. Sci. Eng. A* **2009**, *503*, 185.

[34] B. B. Straumal, S. V. Dobatkin, A. O. Rodin, S. G. Protasova, A. A. Mazilkin, D. Goll, B. Baretzky, *Adv. Eng. Mater.* **2011**, *13*, 463.

[35] M. H. Hong, K. Hono, W. T. Reynolds Jr., T. Tarui, *Metall. Mater. Trans. A* **1999**, *30*, 717.

[36] A. Lamontagne, V. Massardier, X. Kléber, X. Sauvage, D. Mari, *Mater. Sci. Eng. A* **2015**, *644*, 105.

[37] Y. Ivanisenko, R. K. Wunderlich, R. Z. Valiev, H.-J. Fecht, *Scr. Mater.* **2003**, *49*, 947.

[38] H. J. Grabke, W. Paulitschke, G. Tauber, H. Viefhaus, *Surf. Sci.* **1977**, *63*, 377.

[39] J. C. Russ, R. T. Dehoff, *Practical Stereology*, 2nd ed., Plenum Press, New York **2000**, p. 21.

[40] M. Haddad, Y. Ivanisenko, E. Courtois-Manara, H.-J. Fecht, *Mater. Sci. Eng. A* **2015**, *620*, 30.

[41] K. Neishi, Z. Horita, T. G. Langdon, *Mater. Sci. Eng. A* **2002**, *325*, 54.

[42] S. V. Divinski, G. Reglitz, H. Rösner, Y. Estrin, G. Wilde, *Acta Mater.* **2011**, *59*, 1974.

[43] H. K. D. H. Bhadeshia, *Mater. Sci. Technol.* **2015**, *31*, 758.

[44] W. Lefebvre-Ulrikson, F. Vurpillot, X. Sauvage (Eds.), *Atom Probe Tomography, Put Theory into Practice*, Elsevier, Amsterdam, The Netherlands **2016**.

[45] J. L. Burns, *Trans AIME* **1934**, *113*, 239.

[46] I. MacLaren, Y. Ivanisenko, H.-J. Fecht, X. Sauvage, R. Z. Valiev, *Ultrafine Grained Materials IV* (Eds: Y. T. Zhu, T. G. Langdon, Z. Horita, M. J. Zehetbauer, S. L. Semiatin, T. C. Lowe), TMS (The Minerals, Metals & Materials Society), Charlotte, North Carolina **2006**.

[47] C. Borchers, T. Al-Kassab, S. Goto, R. Kirchheim, *Mater. Sci. Eng. A* **2009**, *502*, 131.

[48] W. Guo, Y. Meng, X. Zhang, V. Bedekar, H. Bei, S. Hyde, Q. Guo, G. B. Thompson, R. Shivpuri, J. Zuo, J. D. Poplawsky, *Acta Mater.* **2018**, *152*, 107.

[49] N. I. Medvedeva, L. E. Kar'kina, A. L. Ivanovskii, *Phys. Met. Metallogr.* **2003**, *96*, 452.

[50] G. Langford, *Metall. Trans. A* **1977**, *8A*, 861.